Geoderma 466 (2026) 117685

Contents lists available at ScienceDirect

Geoderma

journal homepage: www.elsevier.com/locate/geoderma

Phosphorus dynamics in acidic and neutral fen soils – does vivianite limit phosphorus release?

Adrian F. Florea [a,*], Dominik H. Zak [b], Rasmus Jes Petersen [b], Carolin L. Dreher [c], Andreas Kappler [c,d], Hans Christian B. Hansen [a]

[a] Department of Plant and Environmental Science, Faculty of Science, University of Copenhagen, Thorvaldsensvej 40, Dk-1871 Frederiksberg C, Denmark
[b] Department of Ecoscience, Aarhus University, C. F. Møllers Allé 3, 8000 Aarhus C, Denmark
[c] Geomicrobiology, Department of Geosciences, University of Tuebingen, Tuebingen, Germany
[d] Cluster of Excellence EXC 2124, Controlling Microbes to Fight Infection, University of Tuebingen, Germany

ARTICLE INFO

Handling Editor: Dr. Andrew Margenot

Keywords:
Peat soil
Anoxic phosphorus release
Iron(III) reduction kinetics
Phosphorus immobilization
Fe(II) phosphate minerals

ABSTRACT

Drainage and cultivation of organic lowland peat soils have profoundly altered their hydrological and biogeochemical functions, increasing greenhouse gas emissions and phosphorus (P) mobilization due to enhanced mineralization. Rewetting is increasingly promoted to mitigate these impacts. However, intensive agricultural use has led to P accumulation, primarily bound to Fe(III)(oxyhydr)oxide minerals, raising the risk of P release under anoxic conditions and challenging the restoration of these systems as nutrient sinks. Predicting P release remains difficult due to complex interactions, including P re-sorption to metal oxides with remaining P binding places and precipitation as Fe(II) or Ca phosphates such as vivianite and hydroxyapatite.

This study investigates Fe(III)(oxyhydr)oxide reduction extent and associated P mobilization in two contrasting Danish lowland peatlands over 24 months: the acidic Vejrumbro and neutral-alkaline Løvenborg. Oxalate-extractable Fe, Al, and P (Fe_{ox}, Al_{ox}, P_{ox}) differed substantially between sites. Løvenborg exhibited higher Fe_{ox} (198–241 mmol kg^{-1}) and Al_{ox} (41–49 mmol kg^{-1}) than Vejrumbro (Fe_{ox}: 27–122 mmol kg^{-1}; Al_{ox}: 4.5–40 mmol kg^{-1}), resulting in greater P sorption capacity (PSC: 239–287 vs. 44–155 mmol kg^{-1}). The degree of P saturation (DPS) remained low at both sites (<10%).

Under winter or wet field conditions, Fe(III)(oxyhydr)oxide reduction extent reached up to 100%, indicating complete dissolution of the Fe_{ox} pool. Despite extensive reduction, soluble P (P_{Sol}) remained low in Løvenborg (≤0.3 mg L^{-1}), whereas Vejrumbro exhibited high P_{Sol} concentrations (up to 4.7 mg L^{-1}). Powder X-ray diffraction and Mössbauer spectroscopy confirmed vivianite formation in Løvenborg, demonstrating P immobilization via precipitation. Moreover, in Løvenborg, the saturation index calculated using the geochemical model Minteq showed values between 2.5 and 4.2 with respect to vivianite supersaturation, while for Ca-P precipitates such as hydroxyapatite, Løvenborg soils show near equilibrium (0.09) to slight undersaturation (−1.8). In contrast, P retention in Vejrumbro was mainly through adsorption onto residual Fe and Al oxide minerals.

These results indicate that P release risk models must go beyond re-adsorption, and include precipitation pathways, which depend on metal-oxide content, cation availability (e.g., Ca^{2+}, Fe^{2+}), pH, alkalinity, and the extent of Fe(III) reduction. Incorporating key geochemical indicators—such as pH, sorption capacity, calcium content, Fe(III) reduction extent, and alkalinity may lead to better classification of peat soils and guide rewetting strategies safeguarding minimal P release.

Abbreviations: Mg_T, Total magnesium (mmol kg^{-1}); Ca_T, Total calcium (mmol kg^{-1}); ρ_b, Soil density (kg m^{-3}); OC, Organic carbon (%); Al_{ox}, Oxalate extractable Al (mmol kg^{-1}); Fe_{ox}, Oxalate extractable Fe (mmol kg^{-1}); P_{ox}, Oxalate extractable P (mmol kg^{-1}, mg kg^{-1}); Fe_T, Total Fe (mmol kg^{-1}); Al_T, Total Al (mmol kg^{-1}); P_T, Total P (mmol kg^{-1}); Al_{CBD}, Bicarbonate-dithionite extractable Al (mmol kg^{-1}); Fe_{CBD}, Bicarbonate-dithionite extractable Fe (mmol kg^{-1}); P_{CBD}, Bicarbonate-dithionate extractable P (mmol kg^{-1}); P_{Sol}, P released to soil solution (mg L^{-1}); P_{mob}, P mobilized (mmol kg^{-1}, mmol L^{-1}); $Fe(II)_{HCl}$, Hydrochloric acid extractable Fe (II) (mmol kg^{-1}); DPS, Degree of P saturation in soils (%); PSC, P sorption capacity of the soils (mmol kg^{-1}); RSC, Residual sorption capacity of the soils (mmol kg^{-1}); TN, total nitrogen; TC, total carbon.

* Corresponding author.
E-mail address: aff@plen.ku.dk (A.F. Florea).

https://doi.org/10.1016/j.geoderma.2026.117685
Received 1 June 2025; Received in revised form 8 January 2026; Accepted 9 January 2026

1. Introduction

Organic lowland peat soil has been significantly altered by centuries of drainage and cultivation, accelerating soil organic matter mineralization and amplifying greenhouse-gas emissions (Leifeld & Menichetti, 2018; Tiemeyer et al., 2016). Rewetting of degraded agricultural peatlands is seen as a key climate mitigation tool, reducing emissions by up to ~20 tons CO_2-eq. ha^{-1} yr^{-1} and reducing agricultural nitrogen losses through denitrification (Kimmel and Mander, 2010; Lamers et al., 2015). However, intensive agricultural use and fertilization have led to mineralization of organic matter and accumulation of phosphorus (P), mainly in the degraded surface soil layer (Shenker et al., 2005; Zak et al., 2008). A significant part of this P is bound to Fe(III)(oxyhydr)oxides (hereafter referred to as Fe(III)-oxides), or Al(hydr)oxide minerals (hereafter Al-oxides), which is usually used for quantifying the P sorption capacity (PSC) of soils including organic-rich wetlands (Lamers et al., 2015; Zak et al., 2010). Under anoxic conditions, reductive dissolution of Fe(III)-oxides significantly reduces PSC and mobilizes P (Heiberg et al., 2010; Prem et al., 2015; Zak et al., 2010). Consequently, rewetting former intensively managed sites can trigger P mobilization and eutrophication in nearby waters (Hoffmann et al., 2012; Wiegman et al., 2022).

Lowland peat soils are estimated to be among the largest contributors to diffuse P loss to surface waters (Kristensen et al., 2021; Smith et al., 2021). Complex interaction of soil biogeochemistry and wetland hydrology may complicate the prediction of P loss from lowland peat soils (Hattermann et al., 2006; Maassen and Balla, 2010). While anoxic conditions can promote the reductive dissolution of Fe(III)-oxides and subsequent P release, several mitigating processes may counteract this mobilization. These include re-adsorption of P to non-reduced Fe(III)-oxides and/or redox stable Al-oxides (Heiberg et al., 2010; Murray and Hesterberg, 2006), precipitation of P as Fe(II)-phosphate (Fe(II)-P) or Ca-phosphate (Ca-P) (Heiberg et al., 2012; Walpersdorf et al., 2013), and biological P uptake by plants and microbial biomass (Zak et al., 2022). Additionally, the availability of labile organic substrate can regulate microbially driven reduction of Fe(III)-oxides, affecting the extent of P release (Craft, 2010; Kjaergaard et al., 2012) (Fig. 1).

Previous studies have linked anoxic P release risk in lowland peat soils to simple geochemical indicators such as total P (P_T) and the degree of P saturation (DPS) (Nürnberg, 1988; Hooda et al., 2000; Weigman et al., 2022). These models suggest higher P release risk with increasing DPS or P_T. Others use Fe:P molar ratios (Fe_T:P_T) or oxalate-extractable Fe and P (Fe_{ox}:P_{ox}) (Geurts et al., 2008; Surridge et al., 2012). In Denmark, P risk screening commonly relies on bicarbonate-dithionite (BD)-extractable Fe:P (Fe_{BD}:P_{BD}) (Forsmann and Kjaergaard, 2014). These tools are useful but incomplete as they do not account for the fate of P after Fe(III)-oxide dissolution including the potential re-adsorption to sorbents such as clays, Al-oxides, or residual Fe(III)-oxides, nor do they consider the precipitation of P with Fe(II) and Ca.

A recent model predicts anoxic P release caused by reductive Fe(III)-oxide dissolution using oxalate-extractable Fe, Al, P and the extent of Fe (III)-oxide reduction, with a ~100 mmol kg^{-1} residual sorption-capacity threshold separating low from high risk (Florea et al., 2024). Risk increases with low PSC, high DPS, and low Al-oxide content. However, the study of Florea et al. (2024) focused on mainly acid to slightly acid soils, while in neutral to alkaline soils, mobilized P may be re-immobilized as Fe(II)–P (e.g., vivianite ($Fe_3(PO_4)_2$ ● H_2O)) or Ca–P (e.g. hydroxyapatite ($Ca_{10}(PO_4)_6(OH)_2$) precipitates, contributing to the long-term P immobilization (Gächter and Müller, 2003) (Fig. 1).

The aim of this study is to evaluate the extent of Fe(III)-oxide reduction in field conditions, quantifying the concomitant P mobilization and identifying the P immobilization processes taking place in two contrasting peat soils, differing with respect to pH, alkalinity and content of Fe- and Al-oxides. The two soils studied are representative of two common classes of fen peat soils – strongly acid and neutral. We hypothesize that P mobilization in peat soils is primarily driven by the extent of Fe(III)-oxide reduction in the soils. However, the net release of P into the aqueous phase is modulated by immobilization processes, including re-adsorption onto remaining metal oxides in acidic soils, and both re-adsorption and precipitation as Ca-P and Fe(II)-P in neutral soils. The specific objectives of the study were to: (i) quantify the extent of Fe (III)-oxide reduction and associated P release under field conditions during a 24-month period; (ii) evaluate the applicability of the laboratory-based P release model developed by Florea et al. (2024) for P release in field settings, and (iii) identify the dominant mechanisms governing P immobilization.

2. Materials and methods

2.1. Soil sampling and sample preparation

The peat soil samples were collected from two field locations in Denmark. One site is in Vejrumbro – Jutland (56°26′18.1″N 9°32′42.7″E), a part of the larger Nørre Å river valley, categorized as a

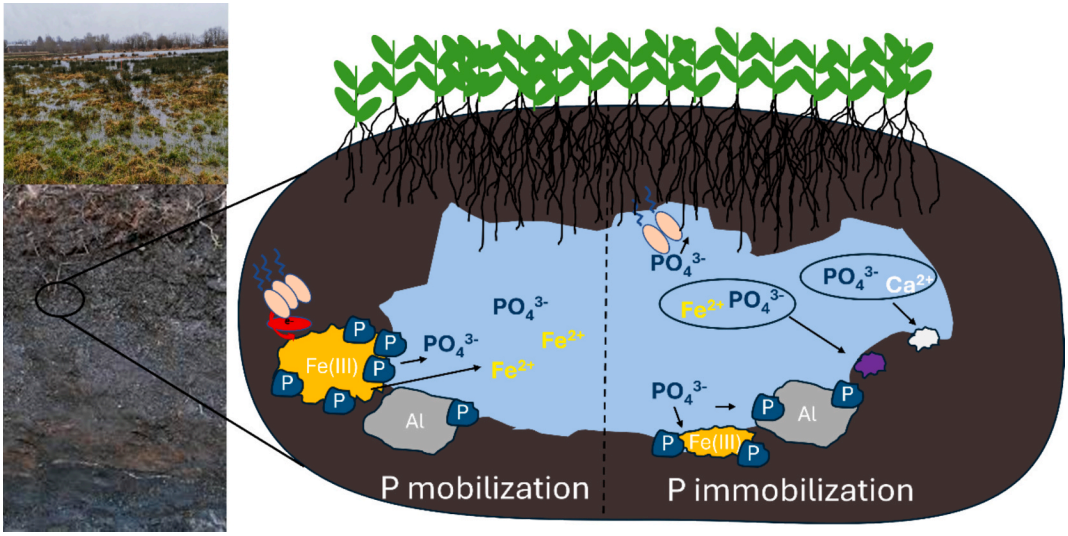

Fig. 1. Schematic illustration of the P mobilization and possible P immobilization processes. Resorption on remaining Fe(III)-oxides and Al-oxides, vivianite precipitation ($3Fe^{2+}(aq) + 2PO_4^{3-}(aq) + 8H_2O \rightleftharpoons Fe_3(PO_4)_2$ ● H_2O and Ca-P ($3Ca^{2+}(aq) + 2PO_4^{3-}(aq) \rightleftharpoons Ca_3(PO_4)_2(s) + 2H_2O$) precipitation. P = bound phosphorus; PO_4^{3-} = released phosphorus; Fe^{2+} = Fe(II) in solution; Ca^{2+} = Ca in solution; ● = vivianite precipitation; ● = Ca-P precipitation.

rewetted riparian fen. The site was ditch drained in the 1950′s and used for grazing purposes. The grazing stopped at the establishment of research infrastructures in the area in 2018. The region has a temperate climate, the annual precipitation is on average 780 mm, and the annual average temperature is 8.5°C. The second site is Located Løvenborg – Zealand (55°41′15.2″N 11°35′22.4″E), where the annual precipitation is on average 700 mm, and annual average temperature is 9°C. The site was historically a grazed meadow until 1975 and later used for production of spring crops (wheat, carrots, potatoes) before being converted to extensively grazed permanent grassland in 2009. Drainage systems, in place since the 1940s, were disabled in 2009, and a dam was established to manage and clean drainage water (e.g. nitrogen removal) from surrounding areas.

The sites were selected based on existing information to cover a large gradient in Al_{ox}, Fe_{ox}, P_{ox}, differences between peat layer thickness and contrasting pH values. The repetitive samples were taken in two soil depths, 0–30 and 30–60 cm, as undisturbed soil cores, using an Eijkelkamp cylindrical, 45-mm diameter soil corer with a sampler liner tube, except where sampling failed due to high groundwater level. A moisture gradient transect was used for soil sampling on both sites. In Vejrumbro, the moisture transect was established across three sampling points (Fig. 2A). Points V1 and V3 represented the driest conditions, while point V2 was identified as the wettest. Topsoil samples (0–30 cm) were denoted as V1T, V2T and V3T, while subsoil samples (30–60 cm) were denoted as V1S, V2S and V3S. The thickness of the peat layer in Vejrumbro field site is around 1.8 m. The distance between the sampling points is 10 m. In Løvenborg, the moisture transect has four collecting points and starts from the wettest point L1 to the driest point L4 (Fig. 2B), with 10-meter distance between the sampling points. Soil samples were collected from a depth of 0–40 cm depth, corresponding to the thickness of the peat layer at this site. Beneath the peat, the subsoil consists of sand (Fig. 2B) (Table S1). Both sites were rewetted, with water tables fluctuating slightly during the monitoring period, from near to above the surface in winter to approximately 30 cm below the soil surface in summer.

The monitoring period covered 24 months from November 2022 to November 2024, with sampling frequency of every 3 months for Vejrumbro and every month for the Løvenborg site, except when sampling failed due to high groundwater level (September–October 2023 in Vejrumbro). Soil classification was done according to IUSS working Group WRB (2022). At Løvenborg, the soil is classified as a Histosol with a sapric nature, based on its highly decomposed organic matter content, with little recognizable plant structure remaining, and dark color. In contrast, the Vejrumbro soil is classified as a Histosol with a fibric nature, based on its slightly decomposed organic materials with recognizable plant structures (Fig. 2).

In the field, samples were immediately packed airtight in plastic bags, transported to the laboratory, and stored at 2°C until further processing. In the laboratory, all work with the moist soil samples was done at 20°C in a Coy anoxic chamber with an atmosphere of 95% nitrogen and 5% hydrogen to avoid oxidation of Fe(II) and other O_2 sensitive substances in the samples. Each moist soil sample was carefully homogenized by hand inside the anoxic chamber. From each soil sample, a representative subsample of 20 g was removed and dried outside the glovebox at 105°C for 24 h to determine soil water content. Another subsample of 20 g was subsequently oven-dried at 40°C for six hours for later oxalate and citrate-bicarbonate dithionite (CBD) soil extraction and analysis. The remaining soil subsample was sealed int an airtight

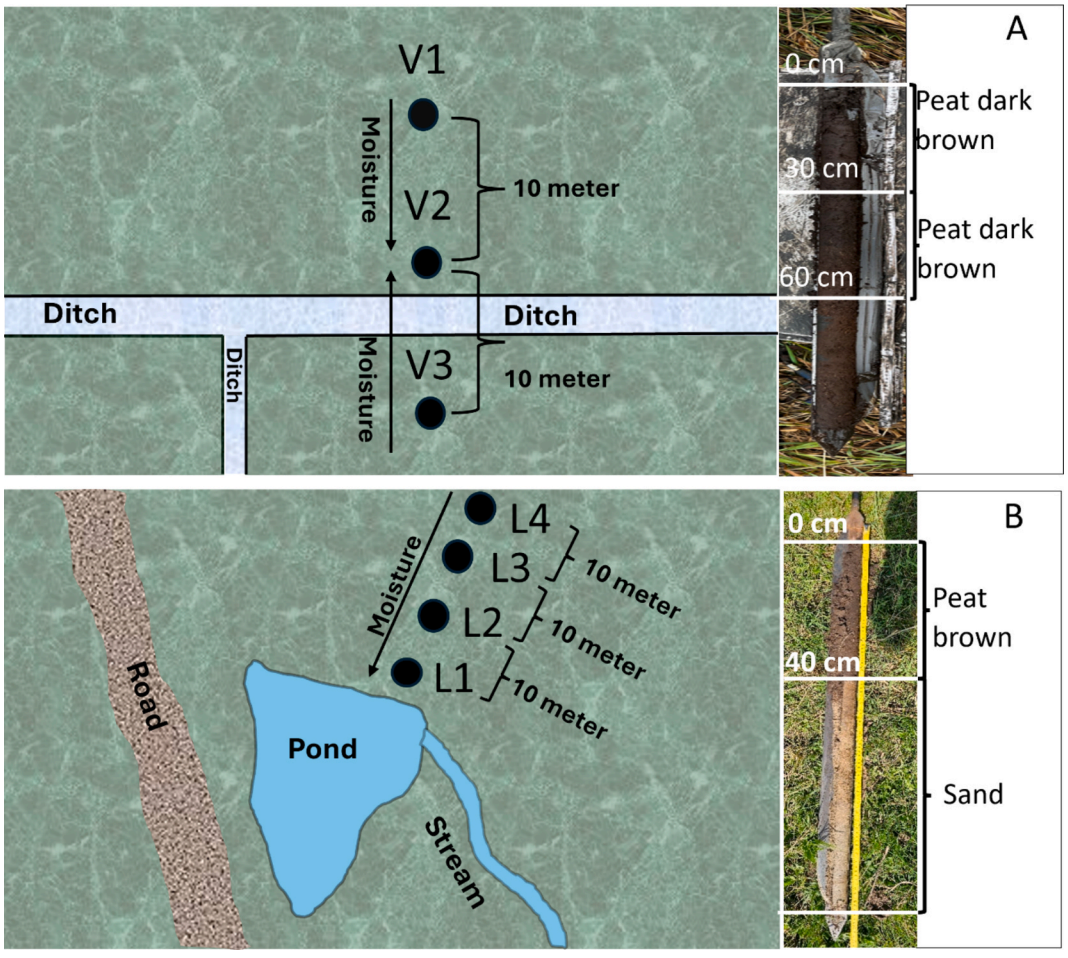

Fig. 2. Sampling transects, moisture gradients, soil profile and peat thickness from both study field sites. A) Vejrumbro, B) Løvenborg.

plastic zip bag and stored moist and anoxic at 2°C in a cooling room until the following day, when analyses of soluble P and HCl-extractable Fe(II) were conducted, if immediate processing on the day of sampling was not feasible. Soil samples dried at 40°C were sieved <2 mm.

2.2. Soil characterization

Orthophosphate in solution was determined by collecting soil solution from the moist soil sample through centrifugation at a 2795 g force, using Chrom-Tech 50 mL PVDF Maxi-Spin 0.45 μm filter tubes (SI – section 2.2). P in solution was determined by spectrophotometry using the molybdate-blue method (ISO, 2004). The P in soil solution was analyzed quickly (within 12 h) after solution sampling to avoid hydrolysis of P bound in organic compounds during the molybdate analysis (Jarvie et al., 2002; Denison et al., 1998). The Fe(II) in solution was analyzed by the 1,10-phenanthroline method of Fadrus and Maly (1975) after appropriate dilutions. pH and electrical conductivity (EC) were measured directly on soil solution, inside the glovebox, immediately after extraction, using a Metrohm 914 portable pH/conductometer, while alkalinity was determined using Gran titration (Gran, 1952).

The extent of Fe(III)-oxides reduction ($R_{Fe(III)}$) in field samples was monitored by determining the content of Fe(II) in soil samples and was calculated as the ratio $Fe(II)_{HCl}$: Fe_{ox} (Eq. (1)) (SI – section 2.2). The Fe(II) in the supernatant determined by the 1,10 − phenanthroline method of Fadrus and Maly (1975). The method is a milder method of Lovley et al. (1987) and aims to extract sorbed and exchangeable Fe(II) as well as Fe(II) in easily soluble mineral phases, such as siderite and vivianite. Moreover, the HCl extract was analyzed for P concentrations using the above-described molybdenum method. The centrifugation method was tested for Fe(II) oxidation during the sample centrifugation, by measuring $Fe(II)_{HCl}$ on several samples, before and after centrifugation. The results showed no significant oxidation of the soil sample during solution extraction by centrifugation outside the glovebox.

$$R_{Fe(III)} = \frac{Fe(II)_{HCl}}{Fe_{ox}} \times 100 \quad (1)$$

Oxalate-extractable Al, Fe and P were determined following Schoumans (2000), and Al, Fe and P in the extract quantified using ICP-OES (Inductively Coupled Plasma Optical Emission Spectrometry) (SI – section 2.2).

We performed a citrate bicarbonate-dithionite (CBD) extraction on oven-dried soil samples (40°C) to quantify extractable Al, Fe, and P (Fe_{CBD}, Al_{CBD}, and P_{CBD}). The extraction was carried out at 70°C in a water bath, following the method outlined by Mehra and Jackson (1960) (SI – section 2.2). All results are reported on a soil dry mass (DM) basis.

Total P content in soils was determined, after hot acid digestion (5 mL of 6 M HCl) of 0.5 g combusted soil at 520°C, by the blue-molybdate colorimetric method. For total C and N, the dry soil samples were analyzed on an Elementar Vario Macro Cube instrument. Total Fe, Al, Ca, Mg elemental composition of the soil samples was done by X-Ray fluorescence spectrometer (XRF) analysis. The dry and manually milled fine particles soil samples using an agate mortar and pestle, were pelletized using a hydraulic press and cellulose binder and were analyzed on an Olympus Delta Premium DP-6000 XRF analyzer. For determination of total cations and anions in soil solutions, the solution was extracted from the soil samples using centrifugation as described above. Total cations in the soil solution were determined using ICP-OES while total anions were determined by ion chromatography using a 930 Compact IC Flex instrument.

The dissolved organic carbon (DOC) was measured in the soil solution collected as explained above and acidified using 20 μL of 2 M HCl mL^{-1} solution. DOC measurements were performed using Shimadzu TOC-L CPH, ASI, TNM-ROHS instrument. Total cations, total anions, DOC determination in soil solution, as well as alkalinity and EC explained above, were measured in soil solution collected by centrifugation from all soil samples collected in wintertime (November 2024).

Geochemical equilibrium modeling was conducted using Visual MINTEQ version 3.1 to simulate aqueous speciation and evaluate mineral saturation states relevant to P dynamics (Gustafsson 2014) (SI – section 2.2). Saturation indices (SI) were calculated for key Fe- and Ca-bearing P including vivianite ($Fe_3(PO_4)_2{\cdot}8H_2O$) ($pK_{sp} = -37.7$) (Allison et al. (1991), and hydroxyapatite ($Ca_5(PO_4)_3OH$) ($pK_{sp} = -44.3$).

2.3. Phosphorus sorption, re-sorption capacity and degree of P saturation

The P sorption capacity (PSC, Eq. 2) in soils was calculated by summing the molar contents of Al_{ox} and Fe_{ox} assuming that P binds equally to the two metal fractions in the soils (van der Zee and van Riemsdijk, 1988; Dari et al. 2018). Following Fe(III)-oxide dissolution, the residual sorption capacity (RSC, Eq. 3) for a sample was determined to assess the residual capacity of the soil to immobilize P by adsorption and was estimated by correcting PSC for Fe(III)-oxide dissolution (=Fe(II) production)(Florea et al. 2024).

$$PSC = AL_{ox} + Fe_{ox}\left(mmol{\cdot}kg^{-1}\right) \quad (2)$$

$$RSC = PSC - FE(II)_{HCl}\left(mmol{\cdot}kg^{-1}\right) \quad (3)$$

The degree of P saturation (DPS) (Nair et al., 2004) was calculated as molar ratio between P_{ox} and the PSC (Eq. 4). The fraction of P associated with Fe(III)-oxides $\left(f\frac{Feox}{Pox}\right)$ was calculated as molar ratio of Fe_{ox} remaining in soil ($Fe_{ox} - Fe(II)_{HCl}$) and the RSC at a timepoint multiplied with P_{ox} corrected for P released to solution, P_{Sol} (Eq. (5)), and assuming equal affinity of Al and Fe oxides for P bonding.

$$DPS = P_{ox}/PSC \times 100 \quad (4)$$

$$F_{P_{ox}}^{Fe_{ox}} = \frac{Fe_{ox} - Fe(II)HCl}{RSC} \times \left(P_{ox} - P_{sol}\right)\left(mmol\,kg^{-1}\right) \quad (5)$$

During reductive dissolution of Fe(III)-oxides, the associated P mobilization (P_{mob}) may occur proportional to the extent of Fe(III)-oxide dissolution and can be calculated as the product of Fe(II) production and the initial P saturation of Fe(III)-oxides (Eq. 6). Hence, P_{mob} represents a theoretical maximum P release to solution. However, in practice, not all mobilized P enters the solution due to retention by residual Fe and Al oxides (RSC) or immobilization through precipitation products formation, and thus the P immobilized (P_{immob}) can be estimated as the difference between P_{mob} and P_{Sol} (Eq. (7)).

$$P_{mob} = Fe(II)_{HCl} \times \frac{P_{ox}}{PSC} \quad \left(mmol\,kg^{-1}\right) \quad (6)$$

$$P_{immob} = P_{mob} - P_{Sol} \quad \left(mmol\ kg^{-1}\right) \quad (7)$$

2.4. X-ray diffraction and Mössbauer spectroscopy

We identified crystalline phases by powder X-ray diffraction (PXRD) using a PANalytical X'Pert Pro MPD (Co-Kα, 40 kV, 40 mA). Field-moist soils, collected in April 2024, were transferred to a glovebox, dried for approximately 24 h, hand-milled (agate), packed and leveled in holders, then scanned continuously from 5 to 90° 2θ (0.02° steps, 10 s $step^{-1}$). To enhance detection of phases such as vivianite, we applied magnetic separation using a Neodium block super-magnet coated with a triple-layer of nickel-copper-nickel (Ni-Cu-Ni) and re-analyzed the magnet-rich fraction (cf. Prot et al., 2019).

For iron phase speciation, ^{57}Fe Mössbauer spectra were collected on four samples (L1, L2, V1T, V1S) (collected in April 2024), used also in XRD analysis. Reduced, wet soils were dried and hand milled in the glovebox, using a mortar and a pestle. Next, the milled and anoxic soil samples were packed into air-tight glass vials to prevent oxidation, and sent to Department of Geosciences, University of Tübingen, Germany. In the laboratory, 100 μg powder was loaded in 1 cm^2 Plexiglas holders and

measured in transmission mode at 77 K and 5 K (WissEl drive; ^{57}Co/Rh source) in a He backflow cryostat. Spectra were calibrated to α-^{57}Fe at room temperature and fitted in Recoil using the Voigt-Based Fitting routine (HWHM fixed at 0.124 mm s^{-1}).

3. Results

3.1. Soil and solution properties

Soil properties measured for samples collected in the beginning of the field monitoring period, differed markedly between sites (Table 1). Løvenborg had higher dry bulk density (305–546 kg m^{-3}), neutral pH (7.2), much greater Fe_{ox} (198–241 mmol kg^{-1}) and Al_{ox} (41–49 mmol kg^{-1}), yielding higher PSC (239–287 mmol kg^{-1}) and a narrow DPS (5–7%). Ca and Mg were also higher at the Løvenborg site (Ca 815–1098; Mg 26–37 mmol kg^{-1}), consistent with its higher alkalinity. Vejrumbro soil was lighter (86–311 kg m^{-3}), acidic (pH 4.5), and with less Fe_{ox} (27–122) and Al_{ox} (4.5–40), and thus lower PSC (44–155) and broader range of DPS (1–7%).

The ratio between Fe_{ox}:Fe_{CBD}, which is a measure of the proportion of poorly crystalline Fe(III)-oxides (Schwertmann, 1964), is ~1 in Løvenborg, except L4, where the Fe_{ox}:Fe_{CBD} was 1.2. This suggests that poorly crystalline Fe(III)-oxides, such as ferrihydrite, represent almost all of the Fe(III)-oxides in most of the soils (Table 1). Ratios higher than 1 may indicate the presence of Fe(II) sulfides (Vodyanitskii et al., 2007). In Vejrumbro, Fe_{ox}:Fe_{CBD} ranged between 0.62 and 1.03.

Soil solutions differed strongly between sites (Table 2). Løvenborg was near-neutral/alkaline (pH 6.8–7.2) with high EC (to 4.9 mS cm^{-1}) and alkalinity 830–930 μM HCO_3^-; Cl^- was higher and Fe^{2+} ranged between 274–380 μM, compared with Vejrumbro where the Fe^{2+} varied between 65–568 μM. Vejrumbro was strongly acidic (pH 4.3–4.6), with lower EC (max 443 μS cm^{-1}) and alkalinity 178–200 μM HCO_3^-; SO_4^{2-} was higher and NO_3^- was generally low except at V1 (up to 195 μM).

Vejrumbro soils V2S and V3T had the highest Ca^{2+} concentrations, 1210 and 1140 μM, respectively, exceeding the Løvenborg Ca^{2+} concentrations range of 582–732 μM.

3.2. Field monitoring

3.2.1. Iron reduction

The $Fe(II)_{HCl}$ contents varied widely throughout the monitoring period at both field study sites, and between collection points along the moisture transects. At both study sites, the extent of Fe(III)-oxides reduction reflects full reduction of the Fe_{ox} pool during the prolonged wet and anoxic winter/spring seasons (Fig. 3). Moreover, in Løvenborg, almost 100% of the $Fe(II)_{HCl}$ produced during these anoxic periods was oxidized during the dry summer period, in all sampling points (Fig. 3A). In contrast, in Vejrumbro, full oxidation of the $Fe(II)_{HCl}$ produced only occurred in V1T, V1S, V3T and V3S points of the transect, with no oxidation of Fe(II) during summer observed at V2T and V2S, where the water level was still above ground (Fig. 3B). At Løvenborg, 100% Fe(III) reduction was observed at the wettest sampling point (L1), whereas at Vejrumbro, complete reduction occurred at both V1 and V2 sampling points.

3.2.2. Phosphorus dynamics

During the monitoring period, P dissolved in soil solution (P_{Sol}) concentrations varied substantially among the two sites and among the sampling points in the transects. The P_{Sol} concentrations were very low in Løvenborg, with values between 0.0 and 0.3 mg L^{-1} (Fig. 3C), compared with Vejrumbro where the P_{Sol} concentrations ranged between 0.1 and 4.7 mg L^{-1} (Fig. 3D).

At the Løvenborg field site a high variation in P_{Sol} was observed over the year, but the highest concentration of P_{Sol}, seen during the wintertime, was still low in contrast to the large extent of Fe(III)-oxide dissolution. Maximum observed P_{Sol} concentrations during the monitoring period in Løvenborg comprised a small percentage, 0.3% of P_{ox} released. The potential P release to solution, expressed as P mobilized (P_{mob}) (Eq. (6)) was consistently much higher than P_{Sol} in Løvenborg soils, suggesting a P immobilization, rather than accumulation in the soil solution (Fig. S1). Comparatively, in Vejrumbro, we observed higher P_{Sol} concentration, and the P_{Sol} values were more related to the extent of Fe(III)-oxide dissolution (Fig. S2), and the maximum observed P_{Sol} concentrations during the monitoring period comprised of 8.6% of P_{ox} released.

Table 1
Properties of all soil sampling points from Vejrumbro and Løvenborg moisture transects.

Measurement	Unit	Løvenborg collection depth 0–40 cm				Vejrumbro: T – topsoil (0–30 cm) and S – Subsoil (30–60 cm)					
		L1	L2	L3	L4	V1T	V1S	V2T	V2S	V3T	V3S
pH[a]	in soil solution	7.1	7.2	6.9	6.8	4.3	4.5	4.4	4.6	4.5	4.4
Dry ρ_b^b	kg m^{-3}	305	416	509	546	269	129	181	85	311	120
TC[c]	mass %	28.4	27.4	27.6	28.1	33.9	39.2	25.1	44.4	44.4	47.1
TN[c]	mass %	2.3	1.9	2.2	2.1	1.5	1.7	2.0	1.1	1.7	1.9
Mg_T^c	mmol kg^{-1}	26	28	30	37	17	23	11	17	13	11
Ca_T^c	mmol kg^{-1}	1098	918	925	815	264	426	471	528	555	499
Al_T^c	mmol kg^{-1}	565	763	666	599	443	106	330	154	187	127
Fe_T^c	mmol kg^{-1}	610	502	548	458	220	139	231	148	125	70
P_T^c	mmol kg^{-1}	37.8	40.2	35.3	36.7	27.5	15.7	12.3	17.2	34.6	16.4
Al_{ox}^d	mmol kg^{-1}	40.7	45.3	44.5	49.4	33.3	23	4.5	17.3	40.1	17
Fe_{ox}^d	mmol kg^{-1}	198.7	241	216.3	203.6	122	40.5	45.3	27.1	67.4	30.6
P_{ox}^d	mmol kg^{-1}	16.5	19.8	13.5	18.5	10.3	2.8	1.7	2.3	10.7	2.1
Al_{CBD}^e	mmol kg^{-1}	39.1	41.8	43.9	31.3	52.1	27.1	52	41.4	56.8	33.9
Fe_{CBD}^e	mmol kg^{-1}	198.1	211	221.7	169.1	130.8	64.4	73.5	37.8	58.8	37.6
P_{CBD}^e	mmol kg^{-1}	16.8	16.8	18.2	11.1	14	8.7	19.2	5	17.1	3
PSC[f]	mmol kg^{-1}	239.3	286	261.1	253.1	155.2	63.5	49.8	44.4	107.5	47.6
DPS[g]	%	7	7	5	7	7	4	3	5	1	4
Fe_{ox}: P_{ox}		12.1	12.2	16.1	11	11.9	14.2	27.1	11.7	6.3	14.4
Fe_{ox}: Fe_{CBD}		1	1.1	1	1.2	0.93	0.64	0.62	0.72	1.1	0.85

[a] – pH has been determined in soil solution.
[b] – Bulk density.
[c] – Total C, N, Mg, Ca, Al, Fe and P.
[d] – Oxalate extractable Al, Fe and P.
[e] – Citrate bicarbonate dithionite extractable Al, Fe and P.
[f] – Phosphorus sorption capacity calculated according to Eq. 3.
[g] – Degree of phosphorus saturation calculated according to Eq. 4.

Table 2
Soil solution composition from all soil sampling points from both study sites (Vejrumbro and Løvenborg). Samples were collected in wintertime, on 5th of November 2024 for Løvenborg and 7th of November for Vejrumbro, for soil solution analysis.

Measurement	Unit	Løvenborg collection depth 0–40 cm				Vejrumbro: T – topsoil (0–30 cm) and S – Subsoil (30–60 cm)					
		L1	L2	L3	L4	V1T	V1S	V2T	V2S	V3T	V3S
pH	in soil solution	6.9	7	6.9	6.8	4.3	4.5	4.4	4.6	4.5	4.4
NO_3^-	μM	8.8	6.5	8.5	8.7	196	133	1.9	4.2	0.3	3.2
SO_4^{2-}	μM	29	32	49	167	161	190	692	703	16	3
Cl^-	μM	1298	1382	1439	1354	790	485	779	731	544	561
HCO_3^-	μM	920	930	870	830	200	192	195	182	187	183
Ca^{2+}	μM	582	732	681	641	569	613	756	1219	1141	787
Mg^{2+}	μM	67	100	59	42						
K^+	μM	25	25	24	19						
Na^+	μM	204	250	297	292						
Fe^{2+}	μM	380	310	376	274	79.6	64.5	293	568	299	285
DOC	mg L^{-1}	54	50	54	48	95	95	73	73	98	98

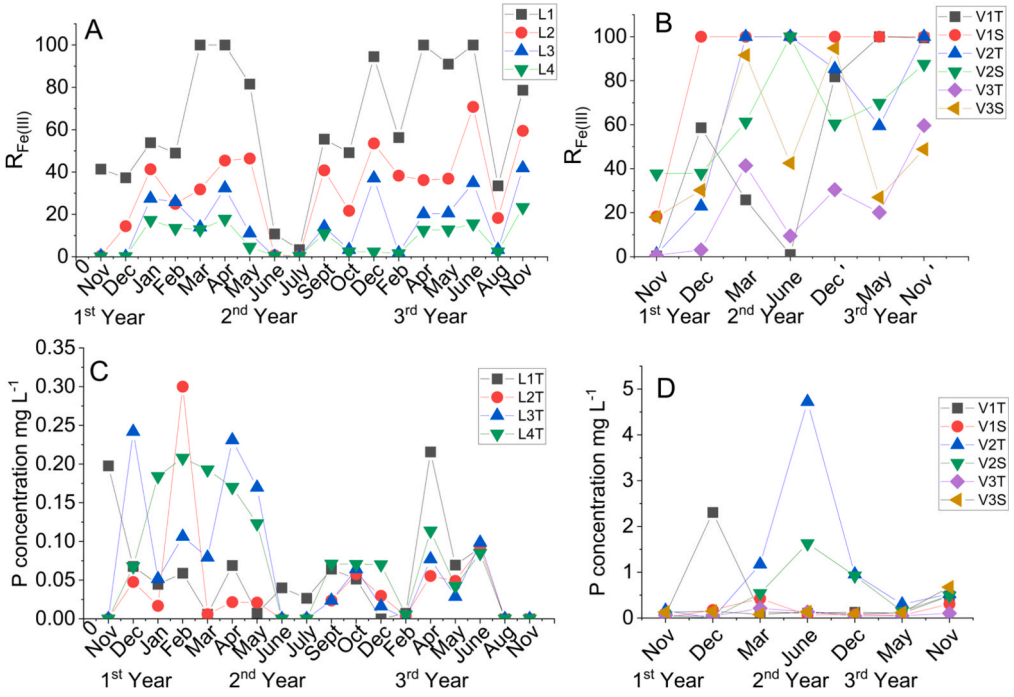

Fig. 3. Extent of iron reduction and soluble phosphorus (P_{Sol}) concentrations at both field sites during the monitoring period. A) Extent of iron reduction ($R_{Fe(III)}$) in Løvenborg during monitoring period. ■ L1 is the wettest point in the sampling transect while ▼ L4 is the driest point in the transect (Fig. 2). B) Iron cycling in Vejrumbro during wet and dry seasons. C) P_{Sol} concentration in mg L^{-1} in field condition for Løvenborg field site during monitoring period. L1 is the wettest point in the sampling transect while ▼ L4 is the driest point in the transect (Fig. 2). D) P_{Sol} concentration in mg L^{-1} in field condition for the Vejrumbro field site. The ''x'' axis represents the sampling time as month and year of soil sample collection. The connecting lines are used as a guide for the eyes to follow the data points.

We analyzed the oxalate extracts using both the molybdate blue method (Wolf and Baker, 1990) and ICP–OES for the L1–L4 samples (Table S2). The comparison shows a close agreement between soluble reactive phosphorus (SRP) determined by the molybdate blue method and total phosphorus measured by ICP–OES. The P_{ox}_molybdate: P_{ox}_ICP ratio averaged 1.08 ± 0.07 (mean ± SD), with individual values ranging from 0.98 to 1.14 (Table S2). This suggests that the oxalate-extractable P pool is predominantly composed of *ortho*-P, while indicating some sample-to-sample variability.

3.3. Solid state analysis

3.3.1. Mineral analysis by X-ray diffraction (XRD)

XRD of the anoxic Løvenborg soil sample L1 collected in April 2024 showed that the soil sample predominantly contained quartz and goethite, and notably, vivianite was also detected in the anoxic soil sample L1. However, in the initial XRD analysis of the untreated soil samples only low-intensity vivianite peaks were detected (Fig. S3), suggesting either a low concentration of vivianite or interference from other soil components. Subsequently, all samples were magnetically treated to preconcentrate vivianite (Nguyen et al., 2024). After magnetic separation, the vivianite peaks became more pronounced and increased in numbers (Fig. 4A). Even if XRD showed vivianite formation in all Løvenborg sampling points, the distribution of vivianite varied spatially (Fig. 4A). L1 and L2 soil samples showed more intense vivianite signals, suggesting more substantial formation of vivianite in these sampling points, while the less wet L3 and L4 exhibited fewer and weaker vivianite signals (Fig. 4A). To further confirm the presence of vivianite, the magnetically separated soil sample L2 was treated with 0.1 M HCl, following the Fe(II) extraction method, and then re-analyzed with XRD. After acid treatment, the vivianite peaks completely disappeared (Fig. S4) supporting the XRD evidence of vivianite in the samples (Zhao et al., 2024).

XRD analysis of soil samples collected from Løvenborg during the

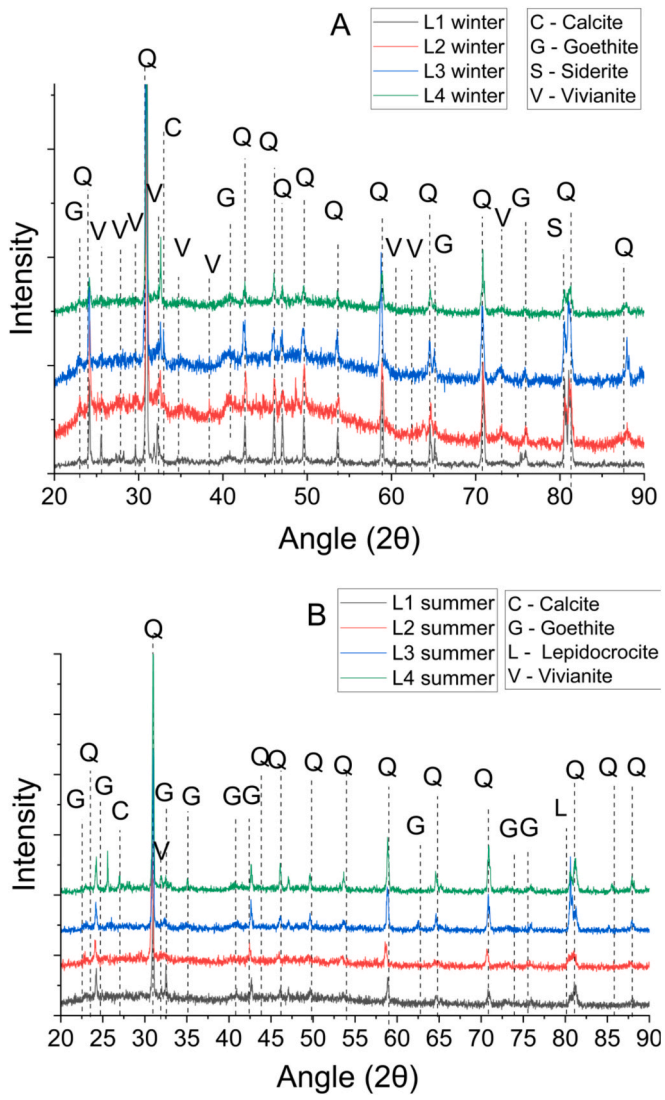

Fig. 4. XRD traces of soil samples collected both in summer and winter. A) anoxic dried and magnetically separated winter soil samples. B) oxic dried and magnetically separated summer soil samples.

summer/dry season, showed that many of the vivianite reflections disappeared, while the remaining vivianite reflections appeared with lower intensity, suggesting a decrease in their overall abundance, or their transformation into other iron minerals under oxidizing conditions. Conversely, goethite peaks became more abundant and prominent (Fig. 4B). Furthermore, in the L1 sampling point, the XRD pattern not only confirmed the presence of goethite but also identified lepidocrocite (γ-FeOOH) (Fig. 4B). The detection of lepidocrocite is indicative of conditions of alternating wetting and drying (Schulz et al., 2023).

The XRD analysis of the anoxic and magnetically treated Vejrumbro soil samples (Fig. S5), showed reflections due to quartz, goethite and lepidocrocite but not vivianite. The diffraction signals corresponding to goethite were relatively broad, indicating a poorly crystalline nature of this mineral. These findings suggest that the crystalline mineral phases in Vejrumbro soil is dominated by quartz, with trace of goethite and lepidocrocite.

3.3.2. *Iron phase characterization by Mössbauer spectroscopy*

Mössbauer spectroscopy revealed a mixture of Fe(III)- and Fe(II)-bearing minerals in all analyzed samples (L1, L2, V1T and V1S), such as poorly crystalline Fe(III)-oxides (L1, L2 and V1T) (Fig. S6; Table 3 and Table S3), Fe(III) bound to silica or to organic matter (all samples) (Fig. S6; Table 3 and Table S3) and vivianite (L2) (Fig. 5A and Table 3).

Sample L2 (collected in April 2024) is taken as an example. The 85% of Fe(III) in this sample can be subdivided into three phases. An Fe(III) doublet still exists at 5 K pointing towards an unordered Fe(III) phase, associated with organic matter or silica (Thompson et al., 2011) (25%). Both the second and third Fe(III) phases are identified as poorly crystalline Fe(III)-oxides based on magnetically ordering of Fe(III) into a defined sextet (Murad and Cashion, 2004) (48%), and Fe(III) ordering into a collapsed feature but without completely magnetically ordering at 5 K (Murad and Cashion, 2004) (12%), respectively (Fig. 5B). The 15% of Fe as Fe(II) in the sample is attributed to vivianite as the two Fe(II) doublets at 77 K have the typical hyperfine parameters for vivianite. Vivianite typically orders into an octet at 5 K, which partly accounts to the area of the collapsed phase (Dyar et al., 2014).

At 77 K, the Fe(II):Fe(III) ratio in sample L1 was 0.87, while in soil sample L2, Fe(III) dominated with an Fe(II):Fe(III) ratio of 0.17, indicating more oxidized conditions in L2. Similarly, V1T showed a higher Fe(II):Fe(III) ratio of 0.82, whereas V1S contained exclusively Fe(III) (100%), confirming a fully oxidized environment (Table 3 and Table S3) (SI). Comparatively, the $R_{Fe(III)}$ was 100% for L1, 45% for L2 and 100% for both V1T and V1S.

4. Discussion

4.1. *Iron reduction*

This study monitored the reduction of Fe(III)-oxides and concomitant P release during 24 months of oxic and anoxic field conditions in two contrasting lowland peat soil sites. The monitoring data highlighted the influence of seasonal fluctuations on the extent of Fe(III) reduction, $R_{Fe(II)}$, with fluctuations spanning the whole range from 0 to 100% both within and between the sites. This means that the full Fe_{ox} pool is cycled during the year, and large amounts of Fe is cycled. For instance, for site L1 it is estimated that the annual cycling of Fe in the upper 40 cm amounts to 13.5 tons ha^{-1} $year^{-1}$. All P associated with this Fe fraction is subject to mobilization and immobilization processes. As an example, under complete reduction of Fe(III)-oxides in the upper 40 cm at sampling point L1, the mobilized P, P_{mob} (Eq. 6), amounts to 13.7 mmol kg^{-1}, and hence leads to P mobilization of 500 kg ha^{-1} $year^{-1}$ (SI – section 4.1). Large amounts of P are being mobilized and subject to potential transport if the P is not re-immobilized.

The Fe_{ox}:Fe_{CBD} ratio, which is a measure of the fraction of poorly crystalline Fe(III)-oxides (Schwertmann, 1964), was always higher than 0.9 (Table 1), reflecting that the poorly crystalline Fe(III)-oxides make up all the oxalate extractable Fe in these samples. This finding is further validated by the XRD analysis of the summer/dry soil samples from these samples, which did not identify crystalline iron minerals. However, we identified broad and low intensity goethite XRD signals, indicating that poorly crystalline or nanocrystalline goethite was formed. The exclusive presence of poorly crystalline goethite in these two samples aligns with the dynamic Fe cycling seen in peat soils, as it forms under low temperature, wet and fluctuating redox conditions (Cornell & Schwertmann, 2003; Hansel et al., 2005). Under these conditions, Fe is repeatedly reduced and re-oxidized, preventing the full crystallization of Fe(III)-oxides and favoring the formation of highly reactive, nanocrystalline goethite (Kappler & Straub, 2005). Moreover, due to its high surface area and great reactivity, poorly crystalline goethite may play an important role in P immobilization and iron cycling in peat soils (Lalonde et al., 2012; Yang et al., 2017).

In contrast to our results, previous laboratory batch experiments have shown that high amounts of soluble Fe(II) could slow down or inhibit the reduction of Fe(III)-oxides, as sorbed or surface-precipitated Fe(II) can limit the potential for enzymatic electron transfer (Roden et al., 2000). However, the inhibiting effect of Fe(II) might be diminished by the subsequent precipitation of minerals like pyrite, vivianite, siderite, or by Fe(II) complexation with organic ligands (Huang et al,

Table 3
Parameters from Mössbauer spectroscopy analysis.

Sample code	Phase	[3]CS (mm/s)	[4]QS/ ε (mm/s)	[5]H (T)	[6]Σ	[7]Relative area (%)	[8]χ^2
L1 (77 K)	Fe(III) doublet	0.50	0.74		0.41	45.7	*0.56*
	Fe(II) doublet	1.29	2.91		0.37	39.6	
	[2]Def. sextet	0.40	−0.07	46.3	5.53	14.7	
L1 (5 K)	Fe(III) doublet	0.65	0.51		0.23	9.4	*0.73*
	Fe(II) doublet	1.34	2.89		0.43	33.9	
	[1]Col. phase	0.60	0	16.09	16.09	33.3	
	[2]Def. sextet	0.50	0	48.46	4.79	23.4	
L2 (77 K)	Fe(III) doublet	0.47	0.79		0.39	85.5	*0.65*
	Fe(II) doublet	1.32	2.60		0	2.3	
	Fe(II) doublet	1.11	3.25		0.69	12.2	
L2 (5 K)	Fe(III) doublet	0.42	0.82		0.49	25.3	*0.75*
	[1]Col. phase	0.50	0	20.0	8.86	26.7	
	[2]Def. sextet	0.47	−0.04	46.95	4.74	48.0	
V1T (77 K)	Fe(III) doublet	0.51	0.94		0.60	55.1	*0.61*
	Fe(II) doublet	1.17	2.72		1.44	44.9	
V1T (5 K)	Fe(III) doublet	0.49	0.97		0.52	39.8	*0.51*
	Fe(II) doublet	1.39	2.81		0.50	14.4	
	[1]Col. phase	0.40	0	28.49	28.49	34.2	
	[2]Def. sextet	0.49	−0.029	50.74	50.74	11.4	
V1S (77 K)	Fe(III) doublet	0.42	0.65		0.33	100.0	*0.68*
V1S (5 K)	Fe(III) doublet	0.46	0.71		0.25	100.0	*0.56*

1 – Collapsed phase: describes a specific structural form of a material.
2 – Refers to a six-line splitting pattern in the spectrum that results from the magnetic hyperfine interaction between the nuclear magnetic moment and an internal magnetic field at the iron nucleus.
3 – Center Shift: measures the difference in nuclear energy levels between the source and absorber; influenced by the **s**-electron density.
4 – Quadrupole Splitting: a key parameter used to interpret the electric field gradient at the nucleus of the Mössbauer isotope (typically ^{57}Fe).
5 – refers to the magnetic hyperfine field at the iron nucleus, measured in tesla (T).
6 – Full Width at Half Maximum (FWHM).
7 – Refers to the proportion of total absorption attributed to a specific spectral component (e.g., Fe^{2+} doublet, Fe^{3+} sextet, etc.) in the fitted spectrum.
8 – chi-squared: a goodness-of-fit statistic used to evaluate how well the model (fit) matches the measured spectrum.

2021; Zak et al., 2010). Thus, dissolved Fe(II) concentrations were low, with a maximum concentration of 380 μM (Table 2) which is unlikely to influence or pose toxicity to microorganisms. The distribution coefficient ($Kd_{Fe(II)}$) calulated based on $Fe(II)_{HCl}$ and Fe(II) measured in solution (Fig. S7) reflects a very strong bonding of Fe(II).

4.2. Phosphorus dynamics

4.2.1. Phosphorus mobilization and release

The soils' PSC varied widely in our study but tended to be higher, compared to PSC values typically measured in soils in Denmark (Møller et al., 2023; Beucher et al. 2020). Previous studies have shown that P_{Sol} in rewetted wetlands can vary largely by one to two orders of magnitude (Zak et al., 2010). During the monitoring period the P_{Sol} concentrations in our soil samples ranged between 0.0 mg L^{-1} and 4.72 mg L^{-1}, showing high variation between winter and summer seasons (Fig. 3). Notably, much higher P_{Sol} concentrations were measured during wet/anoxic periods at the acidic Vejrumbro site, compared to the low concentrations measured at the neutral Løvenborg site. These findings align with previous studies, which concluded that acidic soils may pose a greater risk of P release under anoxic conditions than neutral soils (Amarawansha et al., 2016).

The potential P release to solution, expressed as P mobilized (P_{mob}) is generally much higher than P_{Sol}. As only a small fraction of P_{mob} was measured as P_{Sol}, during the field monitoring period (Fig. S1), a large part of P_{mob} has undergone immobilization. This strongly suggests P resorption onto Al-oxides, remaining Fe(III)-oxides, clays or precipitation as Ca-P or Fe(II)-P minerals (Heiberg et al., 2012; O'Connell et al., 2015; Rothe et al., 2016; Florea et al., 2024). Microbial uptake of P is unlikely to contribute to low P_{Sol} concentrations, as previous experiments found that microbial P uptake generally decreased under anoxic conditions (Gross et al., 2020). In fact, dying and lysis of microbes after rewetting might even contribute to short-term P release (Turner and Haygarth, 2001).

It was found that the relative release of P expressed as P_{Sol}:P_{ox} versus RSC followed the model by Florea et al. (2024) for Vejrumbro soil samples, but not for Løvenborg when extent of Fe(III) reduction is high (Fig. 6). Thus, other P immobilization processes than re-adsorption is active at the neutral Løvenborg, and precipitation of P such as Fe(II) and Ca phosphates should be considered.

4.2.2. Phosphorus immobilization

The good linear correlation (R^2 = 0.78) found between HCl extractable P (P_{HCl}) and $Fe(II)_{HCl}$ (Fig. S8) during the entire monitoring period in Løvenborg suggests that the immobilization of P_{mob} is represented mainly by Fe(II)-P precipitation. Alternatively, Ca-P precipitates might form when P is mobilized during Fe(III)-oxide reduction. However, such precipitates which are insensitive to pH should then persist also under oxic conditions which however does not confer with the low P_{HCl} at low $Fe(II)_{HCl}$. A third explanation is that the mobilized P re-adsorbs to residual Fe(III)-oxides and mainly Al-oxides. But also, in this case this is not supported by the relationship in Fig. S8, as under oxic

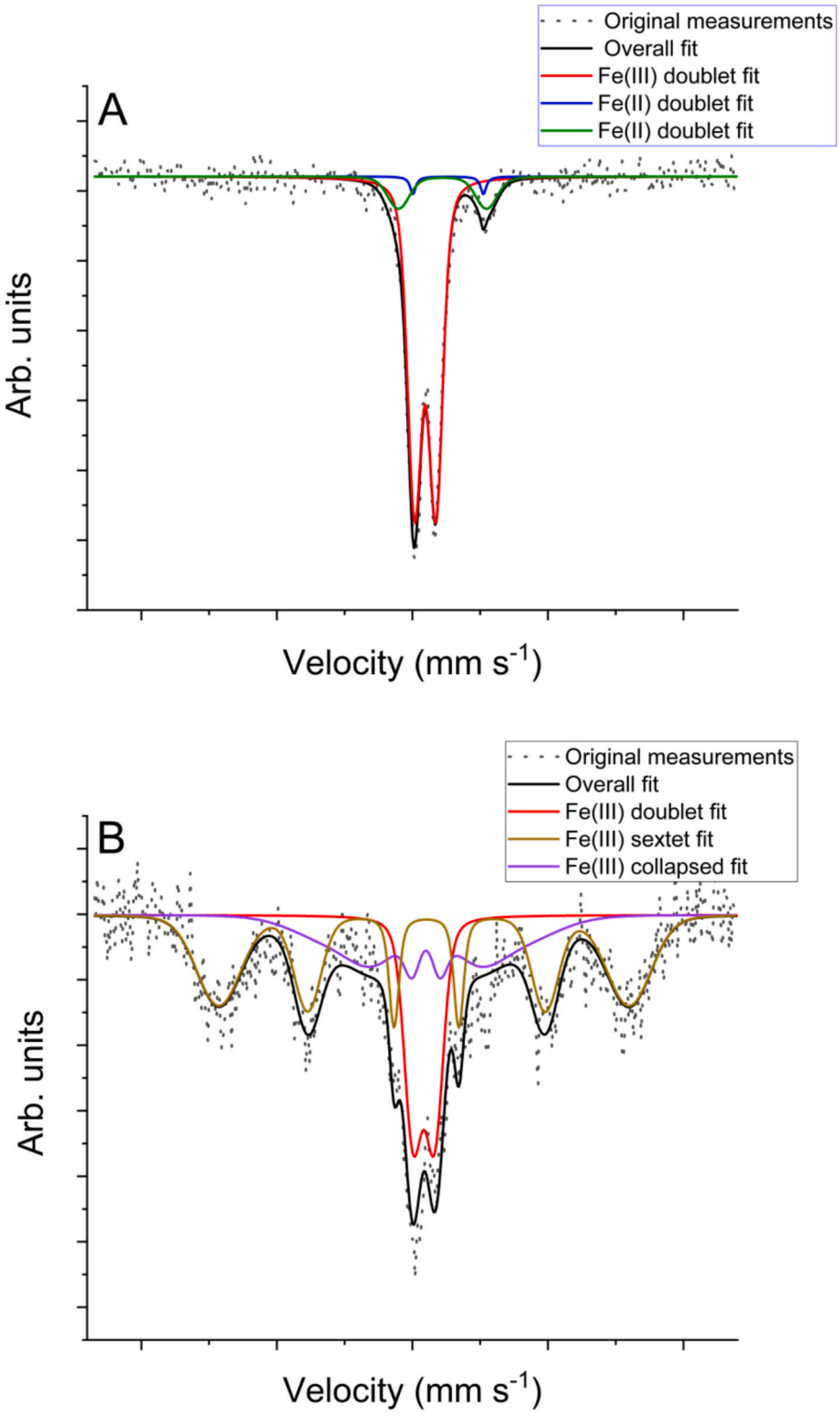

Fig. 5. Example of Mössbauer spectra for Løvenborg soil sample L2. A) This sample is measured at 77 K and was defined by a dominant ● Fe(III) doublet (CS 0.47 mm s^{-1}, QS of 0.79 mm s^{-1}) and two (● and ●) less dominant Fe(II) doublets (CS of 1.32 and 1.1 mm s^{-1}, QS of 2.60 and 3.25 mm/s). B) The 5 K spectra is defined by a dominant ● Fe(III) doublet (CS of 0.42 mm/s and QS of 0.82 mm/s), but also an ● Fe(III) sextet (CS of 0.47 mm s^{-1}. ε of −0.04 mm s^{-1} and H of 46.95 T) and an ● Fe(III) collapsed feature (CS of 0.50 mm s^{-1}, ε of 0 mm s^{-1}, H of 20.0 T). The black dots display the original measurement, and the black line is the overall fit.

conditions (low Fe(II)) P in the soils is not extractable by HCl. Hence, the P_{HCl}-$Fe(II)_{HCl}$ relationships are a strong indication that Fe(II)-P precipitates form. This is supported by both XRD and Mössbauer (Figs. 4 and 5).

For Vejrumbro there is no such correlation between P_{HCl} and Fe $(II)_{HCl}$ as seen in Løvenborg. However, for this soil a reasonable linear correlation ($R^2 = 0.52$) was seen between P_{sol} and $Fe(II)_{HCl}$ (Fig. S1). This suggests that a high amount of the P mobilized from the dissolved Fe(III)-oxide fraction is released to solution, while no P precipitates formed in these samples during the anoxic conditions.

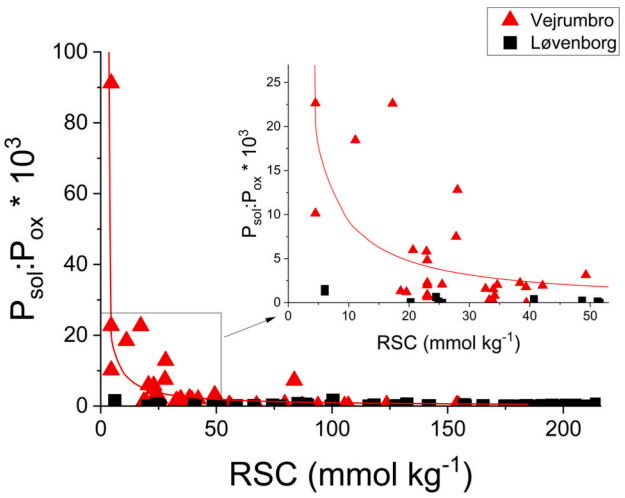

Fig. 6. Relative release of P to solution described as the ratio of soluble P (P_{Sol}) and oxalate extractable P (P_{ox}) (P_{Sol}:P_{ox} (kg L^{-1})) versus the residual sorption capacity (RSC) plotted for all soils and all sampling times. The red line represents the non-linear curve fit in model proposed by Florea et al. (2024).

Vivianite formation in anoxic peat soils is favored by high porewater concentrations of orthophosphate and Fe^{2+} and low levels of sulfide (Nriagu, 1972). The saturation index of the pore water with respect to vivianite, calculated using Minteq and water chemistry values of the measured soil solution, indicates a clear contrast between the two field sites (Table 4). In Løvenborg, the saturation index values between 2.5 and 4.2 reflect high supersaturation with respect to vivianite. For Ca-P precipitates such as hydroxyapatite, Løvenborg soils show weak saturation (0.09) to slight undersaturation (−1.8), meaning hydroxyapatite is marginally stable and could precipitate only under some specific local hot-spot conditions. However, increasing the pH in the Minteq calculations results in increasing the saturation index with respect to both vivianite and hydroxyapatite. A pH increase of 0.1 units will increase the saturation index by 0.5 for hydroxyapatite and 0.2 for vivianite (Fig. S9). Moreover, increasing the P_{sol} concentration with 1 μmol L^{-1} in the calculation, results in an increase of the saturation index for hydroxyapatite by 33% while only 3% for vivianite. Thus, the equilibrium calculations suggest that vivianite-bound P plays a crucial role in P retention in Løvenborg, but hydroxyapatite precipitation cannot be ruled out, as small changes in the pH during the oxic-anoxic transition may lead to Ca-P precipitation.

Vivianite and Ca-P minerals may not show the same precipitation kinetics. Vivianite can precipitate rapidly under anoxic, Fe^{2+}–PO_4-rich, near-neutral conditions (pH 6.5–7.5), often via a nonclassical pathway in which Fe^{2+} and P first produce an amorphous ferrous-phosphate precursor (AFEP) that reorganizes into crystalline vivianite; nucleation and growth rates scale with supersaturation, helping explain fast P capture in suitable field and treatment settings (Paskin et al., 2023). In contrast, hydroxyapatite follows multi-stage kinetics and nucleates faster as pH and alkalinity rise (Reynaud et al., 2022). Thus, field systems may favor one mineral over the other on different timescales even at similar P levels. High Fe^{2+}:P with low sulfide favors vivianite; high Ca^{2+} activity and carbonate alkalinity favor Ca–P. In mixed systems, Ca^{2+} can inhibit or alter vivianite crystallization, shifting P into Ca–P at certain Ca levels and pH. (Hao et al., 2022).

Comparatively, in Vejrumbro, the saturation index reveals strong undersaturation with respect to both vivianite and Ca-P minerals (Table 3) in agreement with no observations of these precipitates at this site.

When exposed to oxygen, vivianite can transform into metavivianite ($Fe(II)Fe(III)_2(PO_4)_2(OH)_2{\cdot}6H_2O$), the amorphous ferric hydroxy phosphate santabarbaraite ($Fe(III)_3(PO_4)_2(OH)_3{\cdot}5H_2O$), or Fe(III)-oxides like lepidocrocite (Rothe et al., 2016; Chiba et al., 2020). This finding is further supported by the solid-state analysis of the soil samples. Vivianite is clearly present at the Løvenborg site during anoxic conditions as seen in XRD and Mössbauer (Figs. 4 and 5) while under oxic conditions vivianite reflections are still visible but of low intensity for the wettest sampling points L1 and L2 (Fig. 4B). This observation aligns with the expectation that during drier, oxygen-rich conditions, vivianite becomes unstable and oxidizes into Fe(III)-bearing minerals that strongly bind P. Metz et al. (2024) showed that vivianite oxidation forms a core–shell structure with an amorphous Fe(III)–phosphate surface, leading to diffusion-controlled oxidation. They also showed that goethite may form (Metz et al., 2024), or secondary amorphous Fe(III)−PO_4 at neutral to alkaline pH in agreement with our observations (Figure, Table).

In summary, the solid-state analysis, solution extraction and HCl extractions data of Løvenborg soil samples clearly highlights the seasonal dynamics of vivianite stability in the soils at the study sites, with evidence of oxidation during the summer months leading to the formation of Fe(III)-oxides. Vivianite precipitation may play a significant role in P immobilization in rewetted soils, with some critical environmental implications. First, P immobilization as vivianite reduces the immediate leaching risk, but the mineral remains reactive within the Fe redox cycle, and keeps P susceptible to seasonal redox fluctuations, potentially resulting in a slow but long-term P release. In contrast, precipitation as Ca–P minerals, such as hydroxyapatite, would likely lead to more permanent P immobilization due to its redox insensitivity. However, if land use transition from agriculture to wetland implies a decrease in pH due to cessation of liming (Metz et al., 2024; Wang and Nancollas, 2008), then both vivianite and Ca-P minerals will dissolve. Thus, the long-term impact of land use changes may shift the system from P retention to P release.

4.3. *Towards a better P release risk assessment model*

Our study evaluating Fe(III)-oxide reduction and associated P mobilization under varying redox conditions in two contrasting lowland peat soils showed that seasonal fluctuations may significantly influence Fe cycling. Substantial Fe(II) production occurring during wet, anoxic periods, followed by oxidation in drier, oxic periods, highlights the potential for both P mobilization and immobilization.

Current P release models, including the Danish model based on Fe_{BD}:P_{BD} ratio (Forsmann and Kjaergaard, 2014), and the recently proposed framework by Florea et al. (2024), primarily focus on relationships between P release and sorption capacity. While our findings align with the refined model by Florea et al. (2024) in the acidic Vejrumbro soils, the clear deviations observed for the neutral Løvenborg soils highlight its limitations. This further highlight the need to integrate key geochemical drivers including pH, Ca^{2+} levels, Fe^{2+} availability, residual sorption capacity, and soil pH buffering capacity to accurately assess P release risk during rewetting. Further, the influence of nitrate, sulfate and

Table 4
Saturation index calculated for vivianite and hydroxyapatite for Løvenborg and Vejrumbro sites using Minteq and the soil solution parameters given previously.

Saturation index	Løvenborg collection depth 0–40 cm				Vejrumbro: T – topsoil (0–30 cm) and S – Subsoil (30–60 cm)					
	L1	L2	L3	L4	V1T	V1S	V2T	V2S	V3T	V3S
Vivianite	4.2	3.5	3.2	2.5	−5.6	−5.7	−13.3	−2.1	−4.7	−4.6
Ca-P (hydroxyapatite)	0.09	−0.1	−1.2	−1.8	−14.4	−13.6	−13	−11.3	−13.9	−13.7

wetland vegetation should also be considered (Zak et al., 2025). A high influx of nitrate helps to maintain Fe(III)-oxides, thereby suppressing P mobilization (Cabezas et al., 2013). Conversely, microbial sulfate reduction leads to formation of insoluble Fe sulfides (FeS) reducing the potential for vivianite formation and potentially leading to P mobilization (Wilfert et al., 2020). Additionally, wetland vegetation may contribute to P retention both through P assimilation and through localized oxidation in the rhizosphere and formation of Fe(III) plaques on root surfaces, which act as strong sinks for P (Hupfer and Dollan, 2003).

Incorporating these drivers into a two-layer framework—screening thresholds (e.g., RSC; Fe pool reactivity) followed by predictive terms (pH, Ca^{2+}, Fe^{2+}, SO_4^{2-}/DOC, alkalinity, vegetation) – should improve P-release risk modelling under dynamic redox. This approach captures both mobilization and immobilization processes.

5. Conclusion

This study examined how seasonal changes affect Fe(III)-oxide mineral reduction and P dynamics in two contrasting lowland peat soils. Anoxic conditions during wet periods have triggered full Fe(III)-oxide reduction, followed by re-oxidation of Fe(II) during dry periods, influencing mobilization of P bound to Fe(III)-oxide fraction, and P immobilization through resorption and precipitation processes. At the neutral Løvenborg site, low P release and vivianite formation indicated strong P immobilization, while the acidic Vejrumbro site showed higher P release and lacked vivianite, relying instead on residual Fe and Al oxides for P retention.

In summary, these results highlight the need to consider not only Fe–P dynamics but also pH, Ca contents, and redox variability when assessing the long-term efficacy of wetland restoration strategies for P retention.

The existing P risk model based on residual sorption capacity (RSC), only partially explained these differences. A refined model incorporating soil pH, Ca, Fe(II), alkalinity, and RSC is proposed to better predict P release risk, especially in wetland restoration. Soils could then be classified into high (acidic, low RSC), intermediate (neutral/alkaline, low RSC), and low (neutral/alkaline, high RSC) P release risk categories. Overall, integrating key geochemical factors is crucial for accurate P risk assessments in restored peatland systems.

CRediT authorship contribution statement

Adrian F. Florea: Conceptualization, Data curation, Formal analysis, Investigation, Methodology, Visualization, Writing – original draft, Writing – review & editing. **Dominik H. Zak:** Writing – review & editing, Writing – original draft, Supervision. **Rasmus Jes Petersen:** Writing – review & editing, Writing – original draft, Formal analysis. **Carolin L. Dreher:** Writing – review & editing, Writing – original draft, Formal analysis, Data curation. **Andreas Kappler:** Writing – review & editing, Validation. **Hans Christian B. Hansen:** Writing – review & editing, Writing – original draft, Validation, Supervision, Project administration, Funding acquisition, Conceptualization.

Declaration of competing interest

The authors declare that they have no known competing financial interests or personal relationships that could have appeared to influence the work reported in this paper. This research was supported by the DFF – Independent Research Fund Denmark (Grant No. 1127-00300B) for the project “Mapping Phosphorus Hot Spots – The Ticket to Carbon Sequestration in Lowland Soils (PhosCarb)”.

Appendix A. Supplementary data

Supplementary data to this article can be found online at https://doi.org/10.1016/j.geoderma.2026.117685.

Data availability

Data will be made available on request.

References

Allison, J.D., Brown, D.S., Novo-Gradac, K.J., 1991. MINTEQA2/PRODEFA2: A geochemical assessment model for environmental systems—Version 3.0 user’s manual (EPA/600/3-91/021). U.S. Environmental Protection Agency, Environmental Research Laboratory, Athens, GA.

Amarawansha, G., Kumaragamage, D., Flaten, D., Zvomuya, F., Tenuta, M., 2016. Predicting phosphorus release from anaerobic, alkaline, flooded soils. J. Environ. Qual. 45, 1452–1459. https://doi.org/10.2134/jeq2015.05.0221.

Beucher, A., Koganti, T., Iversen, B.V., Greve, M.H., 2020. Mapping of peat thickness using a multi-receiver electromagnetic induction instrument. Remote Sens. (Basel) 12, 2458. https://doi.org/10.3390/rs12152458.

Cabezas, A., Gelbrecht, J., Zak, D., 2013. The effect of rewetting drained fens with nitrate-polluted water on dissolved organic carbon and phosphorus release. Ecol. Eng. 53, 79–88.

Chiba, K., Takahashi, M., Ohshima, E., Kawamata, T., Sugiyama, K., 2020. The synthesis of metavivianite and the oxidation sequence of vivianite. J. Mineral. Petrol. Sci. 115, 485–489.

Cornell, R.M., Schwertmann, U., 2003. The Iron Oxides: Structure, Properties, Reactions, Occurrences, and Uses. Wiley-VCH.

Craft, C.B., 2010. Biology of wetland soils. Wetland Soils—Genesis, Hydrology, Landscape and Classification. CRC/Lewis Publishers, Boca Raton.

Dari, B., Nair, V.D., Sharpley, A.N., Kleinman, P., Franklin, D., Harris, W.G., 2018. Consistency of the threshold phosphorus saturation ratio across a wide geographic range of acid soils. Agric. Environ. Lett. https://doi.org/10.2134/age2018.08.0028.

Denison, F.H., Haygarth, P.M., House, W.A., Bristow, A.W., 1998. The measurement of dissolved phosphorus compounds: evidence for hydrolysis during storage and implications for analytical definitions in environmental analysis. Int. J. Environ. Anal. Chem. 69, 111–123.

Dyar, M.D., Jawin, E.R., Breves, E., Marchand, G., Nelms, M., Lane, M.D., Mertzman, S. A., Bish, D.L., Bishop, J.L., 2014. Mössbauer parameters of iron in phosphate minerals: implications for interpretation of Martian data. Am. Mineral. 99, 914–942. https://doi.org/10.2138/am.2014.4701.

Fadrus, H., Maly, J., 1975. [Title not available]. Analyst 100, 549.

Florea, A.F., Heckrath, G., Zak, D.H., Mäenpää, M., Hansen, H.C.B., 2024. Phosphorus release from rewetted agricultural peat soils varies strongly with phosphorus resorption capacity. Geoderma 441, 116739. https://doi.org/10.1016/j.geoderma.2023.116739.

Forsmann, D.M., Kjaergaard, C., 2014. Phosphorus release from anaerobic peat soils during convective discharge: effect of soil Fe:P molar ratio and preferential flow. Geoderma 223–225, 21–32. https://doi.org/10.1016/j.geoderma.2014.01.025.

Gächter, R., Müller, B., 2003. Why the phosphorus retention of lakes does not necessarily depend on the oxygen supply to their sediment surface. Limnol. Oceanogr. 48, 929–933. https://doi.org/10.4319/lo.2003.48.2.0929.

Geurts, J.J.M., Smolders, A.J.P., Verhoeven, J.T.A., Roelofs, J.G.M., Lamers, L.P.M., 2008. Sediment Fe:PO_4 ratio as a diagnostic and prognostic tool for restoration of macrophyte biodiversity in fen waters. Freshw. Biol. 53, 2101–2116. https://doi.org/10.1111/j.1365-2427.2008.02038.x.

Gran, G., 1952. Determination of the equivalence point in potentiometric titrations. Part II. Analyst 77, 661–671.

Gross, A., Lin, Y., Weber, P.K., Pett-Ridge, J., Silver, W.L., 2020. The role of soil redox conditions in microbial phosphorus cycling in humid tropical forests. Ecology 101, e02928. https://doi.org/10.1002/ecy.2928.

Gustafsson, J.P., 2014. Visual MINTEQ, Version 3.1. KTH Royal Institute of Technology, Stockholm.

Hansel, C.M., Benner, S.G., Nico, P., Fendorf, S., 2005. Structural constraints of ferric (hydr)oxides on dissimilatory iron reduction and the fate of Fe(II). Geochim. Cosmochim. Acta 69, 5417–5428.

Hao, X., Yu, W., Yuan, T., Wu, Y., van Loosdrecht, M.C.M., 2022. Unravelling key factors controlling vivianite formation during anaerobic digestion of waste activated sludge. Water Res. 223, 118976. https://doi.org/10.1016/j.watres.2022.118976.

Hattermann, F.F., Krysanova, V., Habeck, A., Bronstert, A., 2006. Integrating wetlands and riparian zones in river basin modelling. Ecol. Model. 199, 379–392. https://doi.org/10.1016/j.ecolmodel.2005.06.012.

Heiberg, L., Pedersen, T.V., Jensen, H.S., Kjaergaard, C., Hansen, H.C.B., 2010. A comparative study of phosphate sorption in lowland soils under oxic and anoxic conditions. J. Environ. Qual. 39, 734–743. https://doi.org/10.2134/jeq2009.0222.

Heiberg, L., Koch, C.B., Kjaergaard, C., Jensen, H.S., Hansen, H.C.B., 2012. Vivianite precipitation and phosphate sorption following iron reduction in anoxic soils. J. Environ. Qual. 41, 938–949. https://doi.org/10.2134/jeq2011.0067.

Hoffmann, C.C., Heiberg, L., Audet, J., Schønfeldt, B., Fuglsang, S., Kronvang, B., Ovesen, N.B., Kjaergaard, C., Hansen, H.C.B., Jensen, H.S., 2012. Low phosphorus release but high nitrogen removal in two restored riparian wetlands inundated with agricultural drainage water. Ecol. Eng. 46, 75–87. https://doi.org/10.1016/j.ecoleng.2012.04.039.

Hooda, P.S., Rendell, A.R., Edwards, A.C., Withers, P.J.A., Aitken, M.N., Truesdale, V.W., 2000. Relating soil phosphorus indices to potential phosphorus release to water.

J. Environ. Qual. 29, 1166–1171. https://doi.org/10.2134/jeq2000.00472425002900040018x.
Huang, J., Jones, A., Waite, T.D., Chen, Y., Huang, X., Rosso, K.M., Kappler, A., Mansor, M.M., Tratnyek, P.G., Zhang, H., 2021. Redox chemistry of iron in natural waters and soils. Chem. Rev. 121, 8161–8233. https://doi.org/10.1021/acs.chemrev.0c01286.
Hupfer, M., Dollan, A., 2003. Immobilisation of phosphorus by iron-coated roots of submerged macrophytes. Hydrobiologia 506, 635–640.
ISO, 2004. Water Quality—Determination of Phosphorus—Ammonium Molybdate Spectrometric Method (ISO 6878). International Organization for Standardization, Geneva.
IUSS Working Group WRB, 2022. World Reference Base for Soil Resources: International Soil Classification System for Naming soils and Creating Legends for Soil Maps, fourth ed. International Union of Soil Sciences, Vienna.
Jarvie, H.P., Withers, J.A., Neal, C., 2002. Review of robust measurement of phosphorus in river water: sampling, storage, fractionation and sensitivity. Hydrol. Earth Syst. Sci. 6, 113–131. https://doi.org/10.5194/hess-6-113-2002.
Kappler, A., Straub, K.L., 2005. Geomicrobiological cycling of iron. Rev. Mineral. Geochem. 59, 85–108.
Kimmel, K., Mander, U., 2010. Ecosystem services of peatlands: implications for restoration. Prog. Phys. Geogr. 34, 491–514. https://doi.org/10.1177/0309133310365595.
Kjaergaard, C., Heiberg, L., Jensen, H.S., Hansen, H.C.B., 2012. Phosphorus mobilization in rewetted peat and sand at variable flow rate and redox regimes. Geoderma 173, 311–321. https://doi.org/10.1016/j.geoderma.2011.12.029.
Kristensen, E., Quintana, C.O., Valdemarsen, T., et al., 2021. Nitrogen and phosphorus export after flooding of agricultural land by coastal managed realignment. Estuar. Coasts 44, 657–671. https://doi.org/10.1007/s12237-020-00785-2.
Lalonde, K., Mucci, A., Ouellet, A., Gélinas, Y., 2012. Preservation of organic matter in sediments promoted by iron. Nature 483, 198–200.
Lamers, L.P., Vile, M.A., Grootjans, A.P., Acreman, M.C., van Diggelen, R., Evans, M.G., Richardson, C.J., Rochefort, L., Kooijman, A.M., Roelofs, J.G., Smolders, A.J., 2015. Ecological restoration of rich fens in Europe and North America: from trial and error to an evidence-based approach. Biol. Rev. 90, 182–203. https://doi.org/10.1111/brv.12102.
Leifeld, J., Menichetti, L., 2018. The underappreciated potential of peatlands in global climate change mitigation strategies. Nat. Commun. 9, 1–7. https://doi.org/10.1038/s41467-018-03406-6.
Lovley, D., Stolz, J., Nord, G., et al., 1987. Anaerobic production of magnetite by a dissimilatory iron-reducing microorganism. Nature 330, 252–254. https://doi.org/10.1038/330252a0.
Maassen, S., Balla, D., 2010. Impact of hydrodynamics (ex- and infiltration) on microbially controlled phosphorus mobility in running-water sediments of a cultivated northeast German wetland. Ecol. Eng. 36, 1146–1155. https://doi.org/10.1016/j.ecoleng.2010.01.009.
Mehra, O.P., Jackson, M.L., 1960. Iron oxides removed from soils and clays by a dithionite-citrate system buffered with sodium bicarbonate. Clay Clay Miner. 7, 317–327.
Metz, R., Kumar, N., Schenkeveld, W.D.C., Obst, M., Voegelin, A., Mangold, S., Kraemer, S.M., 2024. Environ. Sci. Technol. 58, 15321–15332. https://doi.org/10.1021/acs.est.4c04809.
Murad, E., Cashion, J., 2004. Iron oxides. In: Mössbauer Spectroscopy of Environmental Materials and Their Industrial Utilization. Springer, Boston, MA, pp. 159–188. https://doi.org/10.1007/978-1-4419-9040-2_5.
Murray, G.C., Hesterberg, D., 2006. Iron and phosphate dissolution during abiotic reduction of ferrihydrite–boehmite mixtures. Soil Sci. Soc. Am. J. 70, 1318–1327. https://doi.org/10.2136/sssaj2005.0292.
Møller, A.B., Heckrath, G., Hermansen, C., Nørgaard, T., Wollesen de Jonge, L., Humlekrog, M.G.M., 2023. Mapping the phosphorus sorption capacity of Danish soils in four depths with quantile regression forests and uncertainty propagation. Geoderma 430, 116316. https://doi.org/10.1016/j.geoderma.2022.116316.
Nair, V.D., Portier, K.M., Graetz, D.A., Walker, M.L., 2004. An environmental threshold for degree of phosphorus saturation in sandy soils. J. Environ. Qual. 33, 107–113. https://doi.org/10.2134/jeq2004.1070.
Nguyen, H., Prot, T., Wijdeveld, W., Korving, L., Dugulan, A.I., Brück, E., Haarala, A., van Loosdrecht, M.C.M., 2024. Robust magnetic vivianite recovery from digested sewage sludge: evaluating resilience to sludge dry matter and particle size variations. Water Res. 266, 122407. https://doi.org/10.1016/j.watres.2024.122407.
Nürnberg, G.K., 1988. Prediction of phosphorus release rates from total and reductant-soluble phosphorus in anoxic lake sediments. Can. J. Fish. Aquat. Sci. 45, 453–462. https://doi.org/10.1139/f88-054.
Nriagu, J.O., 1972. Stability of vivianite and ion-pair formation in the system $Fe_3(PO_4)_2$–H_3PO_4–H_2O. Geochim. Cosmochim. Acta 36, 459–470.
O'Connell, D.W., Jensen, M.M., Jakobsen, R., Thamdrup, B., Andersen, T.J., Kovacs, A., Hansen, H.C.B., 2015. Vivianite formation and its role in phosphorus retention in Lake Ørn, Denmark. Chem. Geol. 409, 42–53. https://doi.org/10.1016/j.chemgeo.2015.05.002.
Paskin, A., Couasnon, T., Perez, J.P.H., Lobanov, S.S., Blukis, R., Reinsch, S., Benning, L. G., 2023. Nucleation and crystallization of ferrous phosphate hydrate via an amorphous intermediate. J. Am. Chem. Soc. 145, 15137–15151. https://doi.org/10.1021/jacs.3c01494.
Prem, M., Hansen, H.C.B., Wenzel, W., Heiberg, L., Borggaard, O.K., 2015. High spatial and fast changes of iron redox state and phosphorus solubility in a seasonally flooded temperate wetland soil. Wetlands 35, 237–246. https://doi.org/10.1007/s13157-014-0608-0.
Prot, T., Nguyen, V.H., Wilfert, P., Dugulan, A.I., Goubitz, K., De Ridder, D.J., Korving, L., Rem, P., Bouderbala, A., Witkamp, G.J., van Loosdrecht, M.C.M., 2019. Magnetic separation and characterization of vivianite from digested sewage sludge. Sep. Purif. Technol. 224, 564–579. https://doi.org/10.1016/j.seppur.2019.05.057.
Reynaud, C., Thomas, C., Costentin, G., 2022. On the comprehensive precipitation of hydroxyapatites unraveled by a combined kinetic–thermodynamic approach. Inorg. Chem. 61, 3296–3308. https://doi.org/10.1021/acs.inorgchem.1c03884.
Roden, E.E., Urrutia, M.M., Mann, C.J., 2000. Bacterial reductive dissolution of crystalline Fe(III) oxide in continuous-flow column reactors. Appl. Environ. Microbiol. 66, 1062–1065. https://doi.org/10.1128/AEM.66.3.1062-1065.2000.
Rothe, M., Kleeberg, A., Hupfer, M., 2016. The occurrence, identification and environmental relevance of vivianite in waterlogged soils and aquatic sediments. Earth Sci. Rev. 158, 51–64. https://doi.org/10.1016/j.earscirev.2016.04.008.
Schulz, K., Notini, L., Grigg, A.R.C., Kubeneck, L.J., Wisawapipat, W., ThomasArrigo, L. K., Kretzschmar, R., 2023. Contact with soil impacts ferrihydrite and lepidocrocite transformations during redox cycling in a paddy soil. Environ. Sci. Processes Impacts 25, 1945–1961.
Schoumans, O.F., 2000. Determination of the degree of phosphate saturation in non-calcareous soils. In: Pierzynski, G.M. (Ed.), Methods of phosphorus analysis for soils, sediments, residuals and waters. Cooperative Series Bulletin 396 (SERA-IEG-17), North Carolina State University, Raleigh, 31–34.
Schwertmann, U., 1964. Differenzierung der Eisenoxide des Bodens durch photochemische Extraktion mit saurer Ammoniumoxalatlösung. Zeitschrift Für Pflanzenernährung, Düngung, Bodenkunde 105, 194–202.
Shenker, M., Seitelbach, S., Brand, S., Haim, A., Litaor, M.I., 2005. Redox reactions and phosphorus release in re-flooded soils of an altered wetland. Eur. J. Soil Sci. 56, 515–525. https://doi.org/10.1111/j.1365-2389.2004.00692.x.
Smith, G.J., McDowell, R.W., Condron, L.M., Daly, K., Ó hUallacháin, D., Fenton, O., 2021. Reductive dissolution of phosphorus associated with iron oxides during saturation in agricultural soil profiles. J. Environ. Qual. 50, 1207–1219. https://doi.org/10.1002/jeq2.20256.
Surridge, B.W.J., Heathwaite, A.L., Baird, A.J., 2012. Phosphorus mobilization and transport within a long-restored floodplain wetland. Ecol. Eng. 44, 348–359. https://doi.org/10.1016/j.ecoleng.2012.02.009.
Tiemeyer, B., Albiac Borraz, E., Augustin, J., Bechtold, M., Beetz, S., Beyer, C., Drösler, M., Ebli, M., Eickenscheidt, T., Fiedler, S., Förster, C., Freibauer, A., Giebels, M., Glatzel, S., Heinichen, J., Hoffmann, M., Höper, H., Jurasinski, G., Leiber-Sauheitl, K., Peichl-Brak, M., Roßkopf, N., Sommer, M., Zeitz, J., 2016. High emissions of greenhouse gases from grasslands on peat and other organic soils. Glob. Chang. Biol. 22, 4134–4149. https://doi.org/10.1111/gcb.13303.
Thompson, A., Rancourt, D.G., Chadwick, O.A., Chorover, J., 2011. Iron solid-phase differentiation along a redox gradient in basaltic soils. Geochim. Cosmochim. Acta 75, 119–133. https://doi.org/10.1016/j.gca.2010.10.005.
Turner, B., Haygarth, P., 2001. Phosphorus solubilization in rewetted soils. Nature 411, 258. https://doi.org/10.1038/35077146.
van der Zee, S.E.A.T.M., van Riemsdijk, W.H., 1988. Model for long-term phosphate reaction kinetics in soil. J. Environ. Qual. 17, 35–41. https://doi.org/10.2134/jeq1988.00472425001700010005x.
Vodyanitskii, Y.N., Vasil'ev, A.A., Morgun, E.G., et al., 2007. Selectivity of reagents used to extract iron from soil. Eurasian Soil Sci. 40, 1076–1086. https://doi.org/10.1134/S1064229307100055.
Walpersdorf, E., Koch, C.B., Heiberg, L., O'Connell, D.W., Kjaergaard, C., Hansen, H.C.B., 2013. Does vivianite control phosphate solubility in anoxic meadow soils? Geoderma 193, 189–199. https://doi.org/10.1016/j.geoderma.2012.10.003.
Wang, L., Nancollas, G.H., 2008. Calcium orthophosphates: crystallization and dissolution. Chem. Rev. 108, 4628–4669. https://doi.org/10.1021/cr0782574.
Wiegman, A.R.H., Myers, G.H., Augustin, I.C., et al., 2022. Potential for soil legacy phosphorus release from restored riparian wetlands within an agricultural landscape. Biogeochemistry 161, 137–156. https://doi.org/10.1007/s10533-022-00972-2.
Wilfert, P., Meerdink, J., Degaga, B., Temmink, H., Korving, L., Witkamp, G.J., Goubitz, K., van Loosdrecht, M.C.M., 2020. Sulfide-induced phosphate release from iron phosphates and its potential for phosphate recovery. Water Res. 171, 115389. https://doi.org/10.1016/j.watres.2019.115389.
Wolf and Baker, 1990. Colorimetric method for phosphorus measurement in ammonium oxalate soil extracts. Commun. Soil Sci. Plant Anal. 21, 2257–2263.
Yang, S., Wu, J., Tan, S., Wang, L., Jiang, L., 2017. Iron oxides and their role in organic carbon preservation in soils. Soil Biol. Biochem. 107, 60–68.
Zak, D., Gelbrecht, J., Wagner, C., Steinberg, C.E.W., 2008. Evaluation of phosphorus mobilization potential in rewetted fens by an improved sequential chemical extraction procedure. Eur. J. Soil Sci. 59, 1191–1201. https://doi.org/10.1111/j.1365-2389.2008.01081.x.
Zak, D., Wagner, C., Payer, B., Augustin, J., Gelbrecht, J., 2010. Phosphorus mobilization in rewetted fens: the effect of altered peat properties and implications for their restoration. Ecol. Appl. 20, 1336–1349. http://www.jstor.org/stable/25680382.
Zak, D., Maagaard, A.L., Liu, H., 2022. Restoring riparian peatlands for inland waters: A European perspective. In: Mehner, T., Tockner, K. (Eds.), Encyclopedia of Inland Waters, 2nd ed. Elsevier, pp. 276–287. https://doi.org/10.1016/B978-0-12-819166-8.00127-4.
Zak, D., Petersen, R.J., Hoffmann, C.C., Audet, J., Carstensen, M.V., Andersen, H.E., Hansen, H.C.B., 2025. Nutrient cycling in wetlands. In: Routledge Handbook of Wetlands. Routledge, p. 94.
Zhao, Y., Korving, L., Grönfors, O., Prot, T., Suopajärvi, T., Luukkonen, T., Liimatainen, H., 2024. Acid leaching of vivianite separated from sewage sludge for recovering phosphorus and iron. Water Res. 266, 122361. https://doi.org/10.1016/j.watres.2024.122361.